CHARACTERIZATION OF SOME YELLOWSTONE GEYSERS' ERUPTIONS USING INFRASOUND

by

AIDA QUEZADA-REYES

Independent Study

Submitted in Partial Fulfillment
of the requirements of the Degree of

Masters of Science in Geophysics

Department of Earth and Environmental Science
New Mexico Institute of Mining and Technology

Socorro, New Mexico

December 2012

ABSTRACT

Geysers are springs that intermittently erupt hot water and steam. As with volcanoes, infrasonic airwaves produced by different geysers provide information about the processes that occur near the nozzle, such as the amount of fluid released during eruptive episodes. The aim of this study was to investigate the acoustic sources corresponding to a diverse variety of geyser behaviors including those at Lone Star, Sawmill and Great Fountain geysers, Yellowstone National Park, Wyoming. Acoustic signals were measured by arrays of microphones deployed around Lone Star and Great Fountain geyser between August 9th to 14th, 2011, and during one hour on August 16th, 2011 at Sawmill Geyser. Infrasound was analyzed with coincident video recordings to quantify and compare the pressure fields generated during explosive phases at the three geysers. I propose that the periodic infrasound recorded at Sawmill, which is dominated by energy at 1 to 40 Hz, is generated by: 1) the formation of steam-filled bubbles and 2) their subsequent bursting at the free surface resulting in a violent steam and water discharge. At Lone Star geyser, where ~18 m/s eruption jets endure for about 25 minutes, sound is dominated by higher frequency infrasound and audio-band signal evolving from 20 – 60 Hz to 40 – 85 Hz. I suggest that the infrasound tremor amplitudes are related to the transition of the erupted two-phase mixture from mostly water (low acoustic radiation) to steam (high acoustic radiation). At Great Fountain I observed three explosive bursts of water and steam during the last stage of the August 11 eruption with

bi-modal infrasound pulses of up to 0.7 Pa-m. I model these pulses as volumetric sound sources and infer up to 32 m^3 of fluid ejection. The variety of recordings reflects the different eruption mechanisms at these geyser systems. Better understanding of the mechanisms of geyser infrasound radiation may help to understand infrasound analogues from erupting silicic volcanoes, which are considerably more difficult to study at close distances.

Keywords: Infrasound; geyser eruption; Yellowstone geysers; jet noise.

ACKNOWLEDGEMENTS

I would like to thank Dr. Jeffrey Johnson for his guidance, dedication, and continual financial support throughout this process. I would also like to thank Dr. Richard Aster for his help, and support for the completion of this work. Dr. Rene Arechiga, Dr. Phil Kyle, and Dr. Glenn Spinelli for their input to this research and manuscript. Dr. Gary Axen and Dr. Lorie Liebrock for their assistance in this process. I am indebted to Dr. Nick Varley for his financial and academic support, time, and friendship during my fieldwork in Mexico.

This work would not have been possible without the contributions from a number of people whose enthusiasm and expertise were very helpful to me during this project. This data was collected as part of the NMT Geophysical Field Methods course held in Yellowstone National Park (2011). I would like to acknowledge Dr. Jeffrey Johnson, who organized the field experiment that collected the acoustic and video data. Dr. Johnson was also largely responsible for the data processing. Discussions with him led to many of the ideas presented in this work, and he was responsible for the revision of the first draft of this document.

I thank the students from the volcano geophysical field methods course: J.Anderson, R.Anthony, A. Curtis, N. Iverson, R. Johnson, D. Kerzni, and M. Sciotto, for

the deployment, maintenance, and retrieval of the infrasonic equipment. Thanks also to the staff at Yellowstone National Park.

I am also grateful to Dr. Mark Murray for the GPS surveying of the geysers and microphone arrays, Dr. Michael Hargather for his time and fruitful discussions related to underwater explosions. Dr. Omar Marcillo for revising and commenting on the first draft of this document and for his continuous assistance with MATLAB coding.

I am grateful to Pat Valentine and Leigh Davidson, whose help and warmth accompanied me throughout my stay at Tech. Thanks to Eric J. Weiss for all his help with software and hardware issues every time I showed up at his door.

I would like to thank my fellow graduate students and friends Omar Marcillo, Laura Rosales Lagarde, Jesus Gomez, Maya El Hariri, and Carlos Ramirez for their continuous support and encouragement inside and outside from Tech. I will be eternally in debt with you, guys!

Thanks to Dr. Xyoli Perez Campos, my spiritual sensei, for always believing in me, and for continuously providing me with the strength to fight for what I wanted.

Special thanks to my family and friends for their endless supply of love, support and encouragement despite the distance. Thank you all for your faith in me.

Finally, to my beloved Tim, my best friend. This work was completed because of your support.

This research was funded by NSF EAR # 0838562.

TABLE OF CONTENTS

Page

LIST OF FIGURES

Page

LIST OF TABLES

Page

This Independent Study is accepted on behalf of the
Faculty of the Institute by the following committee:

Rick Aster, Advisor Date

Rene Arechiga, Committe Member Date

Glenn, Spinelli, Committee Member Date

I release this document to the New Mexico Institute of Mining and Technology.

Aida Quezada-Reyes Date

1. INTRODUCTION

In the last decades, infrasonic waves (sound waves in the range of 0.2 to 10 Hz) have been studied to better understand the physics of sources generated at or near the solid Earth-atmosphere boundary (Garces, et al., 1998; Drob and Picone, 2003; Arrowsmith et al., 2010, Marcillo and Johnson, 2010), as a consequence of natural processes and man-made events. Among these phenomena, underground nuclear tests and mining explosions can be considered as man-made sources, whereas oceanic waves, volcanic explosions, earthquakes, and meteors are examples of natural sources that generate infrasound (Arrowsmith et al., 2010). Another type of a natural source of infrasound is related to geyser activity. When a geyser erupts, it generates pressure waves in the near-infrasound band (1 – 20 Hz) as high-velocity emissions of water and steam find their way out from the vent.

Geysers may be regarded as analogues for volcanoes due to their similarities in seismicity, mass recharge to the system, and eruption dynamics (Kieffer, 1984). These phenomena facilitate detailed studies on recharge and eruptive processes (e.g. Kieffer, 1984; Kedar et al., 1996; Kedar and Kanamori, 1998), some of which would be difficult to perform on most volcanoes (Hutchinson, et al., 1997).

The sound generated by the different types of geyser eruptions may also have analogies with the sound generated by eruptions observed at volcanoes (e.g. Vergniolle and Brandeis, 1996; Johnson and Lees, 2000; Rowe et al., 2000; Johnson et al., 2004;

Garces et al., 2003; Ripepe et al., 2007). Even though the amplitudes of the sound waves from geysers encompass a few tenths of Pa to a few Pa when reduced to 1 m, much of the energy released by these geologic features is related to multiphase fluid dynamic processes similar to those present at some volcanoes.

Towards the goal of better understanding geyser dynamics using infrasound, I investigated and compared the characteristics of three different types of eruptive behavior recorded from fountain-type (Great Fountain and Sawmill), and cone-type (Lone Star) geysers. Three infrasound arrays were deployed on these geysers located at Yellowstone National Park, Wyoming, USA. The spectral content, acoustic energy, and waveform characterization from each eruptive episode were analyzed and compared against each other, and against video recordings of the eruptions when possible. Based on my results, I propose a source model explanation for the activity observed at Sawmill and Lone Star geysers. Volume estimations from pulses generated by ejected material during the final stage from the August 11, 2011, Great Fountain eruption, are also addressed in this work.

2. BACKGROUND

Geysers are rare geologic features. Over one-half of the world's geysers (about 500 active geysers) are located within the boundaries of Yellowstone National Park, Wyoming, turning it into the largest geyser field on earth (Bryan, 2008). Here, the geysers are commonly found scattered among hot springs in ten major areas known as geyser basins.

Geysers consist of a special plumbing system where hydrothermal explosions occur continuously or intermittently as surface water enters in contact with hot rocks. The temperature of the pressurized water rises until it reaches the boiling point. Then, a mixture of superheated water and expanding steam is suddenly ejected into the air. No two geysers are alike. However, they can be classified into cone-type geysers or fountain-type geysers according to their eruption style, which depends to a great extent on the volume of water, the size of the constrictions, and geometry of the plumbing system (Bryan, 2008). The cone-type geysers erupt as a steady, sometimes tall, column of a mixture of jetted water and steam (Rinehart, 1970). The vent is often surrounded by mounds or cones of sinter, hence the name. In contrast, the fountain-type geysers erupt continuous bursts of water from open pools as steam bubbles rise through them and up to the surface (Rinehart, 1970), creating a splashing that differs considerably from the jetting observed at the cone-type geysers.

In the following subsections, the activity and general characteristics of Sawmill, Great Fountain and Lone Star geysers will be addressed.

2.1 Sawmill Geyser

Sawmill Geyser, located in the Upper Geyser Basin (Figure 1a), is part of one of the most active groups of geysers in Yellowstone: the Sawmill Geyser Complex. Sawmill is a fountain-type geyser that erupts bursts of water continuously out of its 1.6 m-nozzle. Each eruption often lasts from 30 to 50 minutes, up to 4 hours, with intervals of 1 to 3 hours between eruptions (Bryan, 2008). During an eruption, the spinning water in the crater reaches heights between 1 to 10 m.

2.2 Great Fountain Geyser

Great Fountain Geyser is a fountain-type geyser located at Lower Geyser Basin (Figure 1a). According to Bryan (2008), once an eruption begins, violent surges of boiling water and steam leave the ~ 4.8 m vent and reach heights of up to 45 m for several minutes. The activity then pauses and resumes after a few minutes. This behavior is often repeated four times within a 45 – 120 minute interval with surges decreasing gradually in height. Bryan (2008) and Johnson et al. (subm) observed that Great Fountain's eruptions occur every 8 to 17 hours.

2.3 Lone Star Geyser

Lone Star Geyser, located in Third Basin (Figure 1a), is one of the biggest in Yellowstone with a 2.7 meter-high geyserite cone and nearly vertical sides. This cone-

type geyser has eruption intervals often close to 3 hours. The main eruption is preceded by a minor play 25 to 35 minutes before (Bryan, 2008). The activity consists of a 30-minute 14-m high eruption that starts with continuous splashing gradually transitioning into a jet of a water-steam mixture, and eventually into a pure-steam jet towards the end of the eruption.

3. EXPERIMENT

Three acoustic arrays were deployed to detect and monitor infrasound generated by active geysers located at Upper, Lower, and Third Geyser Basins, in Yellowstone National Park, (Figure 1a). The first array (GRF) was deployed ~180 m East of Great Fountain geyser at an elevation of 2238 m asl. The second array (YLS), was located ~81 m NW from Lone Star geyser at 2354 m asl, whereas the third array (YSM) was deployed ~ 16 m away from Sawmill geyser at 2236 m asl. Distances are measured from the center of the nozzle of each geyser to the center of its corresponding array.

The sites selected for this experiment required vegetated areas and environments where noise, mostly generated by heavy transit, tourist activity and winds, remained at low levels throughout the day. Each array consisted of four custom-built infrasound sensors deployed at ground level. The infrasound sensors feature AllSensors^{TM} MEMS transducers with a linear dynamic range of -124.5 to +124.5 Pa, and have a flat response between 0.01 to 40 Hz (Marcillo et al., 2012). The sensors from the arrays deployed at Great Fountain and Lone Star geysers were spatially distributed in the following way: one sensor was located at the center of the array while another was oriented radially with respect to the geyser. The other two were spread ~ 30 m away from the central sensor with azimuth angles at 120 and 240 degrees (Figure 1c,d). Cables connected all sensors to a 24-bit resolution Reftek RT130 Digital Acquisition System (DAS) located at the center of the array. Data at both infrasonic arrays were recorded at 1000 Hz, in continuous

mode, and synchronized using GPS timing. Both arrays operated autonomously with two 70 Ah batteries per array from August 9th to August 13th, 2011. Johnson et al. (subm) discuss the arrays' response and precision characteristics in detail.

The array at Sawmill consisted of two microphones deployed SW and NE of the vent (Figure 1e). This array also operated with two 70 Ah batteries, and recorded continuously at 1000 Hz for one hour, starting at 15:25:50 (UTC), on August 16, 2011.

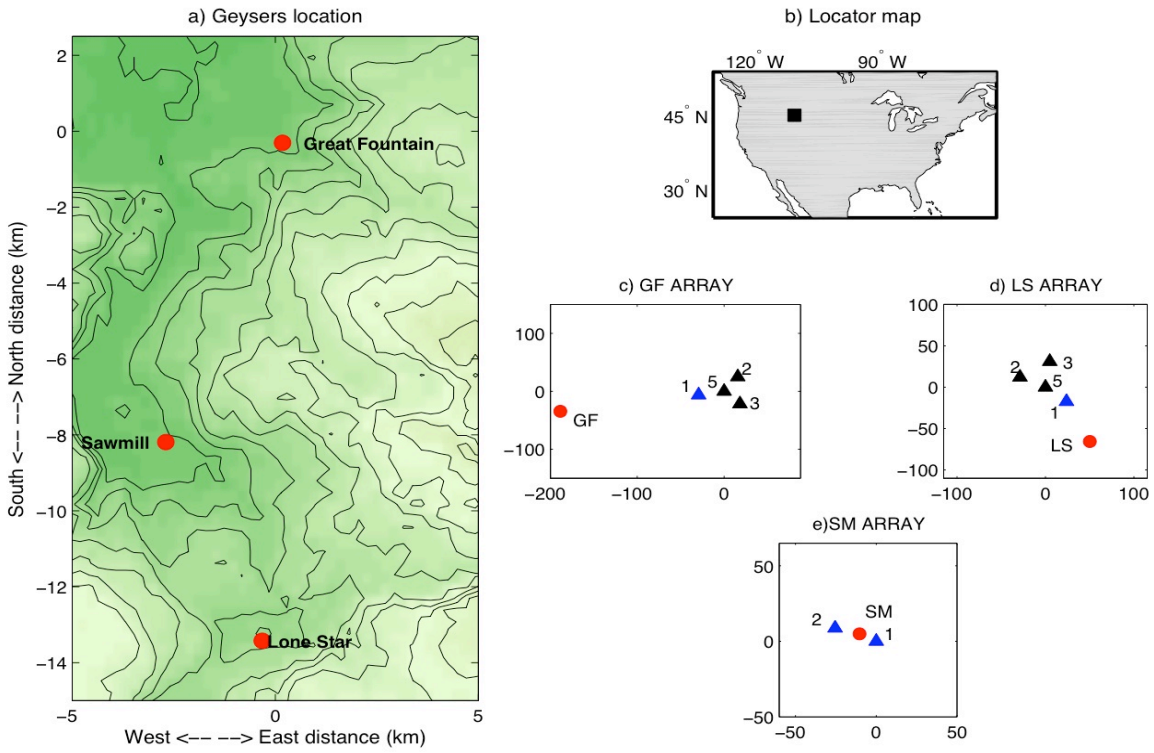

Figure 1. a) Map of geysers located at Upper, Lower and Third Basins, Yellowstone National Park, WY. Fountain, Sawmill and Lone Star geysers are shown in red. b) Location of Yellowstone National Park. c-e) Array geometry with respect to each geyser.

In addition to infrasound, video recordings of the 1-hour activity at Sawmill were made continuously with a camera located ~10 m away from the vent. For Great Fountain, about 30-minute length videos were taken during eruptive episodes on August

9, 10, and 15. Two whole eruptions on Lone Star geyser were also recorded on video on August 9, and 14 with a camera located at a distance of ~ 64 m from the vent and ~68 m from the YLS array. All videos were recorded with a 30 frames-per-second high-resolution Casio Exilim EX-F1 camera.

4. INFRASOUND OBSERVATIONS FROM LONE STAR, GREAT FOUNTAIN, AND SAWMILL GEYSERS

In this section I provide a description and a comparison of the occurrence, waveforms, and spectral content of the sound generated during the eruptive activity recorded at Lone Star, Great Fountain and Sawmill geysers.

Table 1. Events from Lone Star and Great Fountain geysers recorded at infrasound arrays from August 9 to August 14, 2011.

Lone Star geyser			
Day	**Time HH:MM (UTC)**	**Day**	**Time HH:MM (UTC)**
August 9	20:36	12	02:25
	23:08		05:51
10	02:37		09:01
	05:51		11:43
	08:50		14:52
	11:45		17:31
	14:32		20:15
	16:59		23:03
	19:44	13	01:32
	22:37		04:42
11	01:29		08:05
	04:59		11:18
	08:18		14:16
	11:10		17:01
	14:18		19:29
	17:45	14	16:21
	20:46		
	23:18		
Great Fountain geyser			
10	02:24	12	00:40
	14:10		16:11
11	01:57	13	10:29
	13:03		

Table 1 displays a total of 34 and 7 eruptive events from Lone Star and Great Fountain geyser respectively with clearly visible atmospheric pressure perturbations recorded at their corresponding infrasound arrays, from August 9 to 14, 2011.

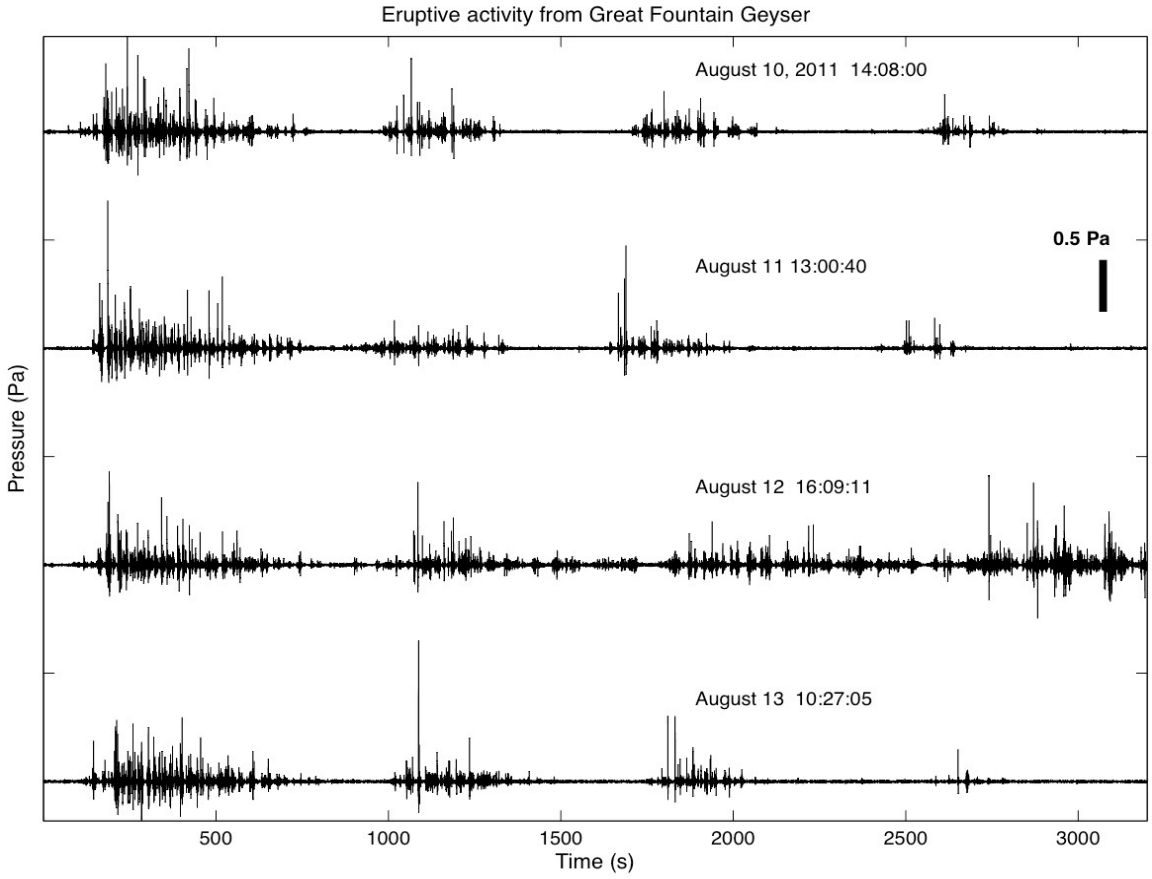

Figure 2. Acoustic traces for four eruptive events from Great Fountain recorded at YGF array between August 10 – 13, 2011. Waveforms are reduced to 1 m. Amplitudes are indicated by the scale bar located on the right hand side of the figure.

Excess pressure recorded from the eruptions observed at Great Fountain (Figure 2) displays four series of pulses that decrease in amplitude until they reach background noise levels for approximately 200 s (quiet phase). The series of pulses resumes right after the quiet phase; however, the amplitude of the pulses decreases considerably after each series towards the end of the eruption.

Infrasound generated at Lone Star geyser differs from that observed at Great Fountain and Sawmill geysers. The 24-hour infrasound recorded at YLS (~81 m) from August 11 (Figure 3) shows Lone Star geyser's typical daily activity. The ~ 25-minute, emergent cigar-shaped waveforms from the eruptions reached amplitudes of up to 0.07 Pa during the most intense phase. These events can be observed at ~3 hour intervals starting at 1:29:00 (UTC) (see Table 1). The high-amplitude pulsing signal visible from 4:00 PM to 12:00 AM, on August 11th, and also apparent on August 9, 10, 12, 13 and 14, is due to winds.

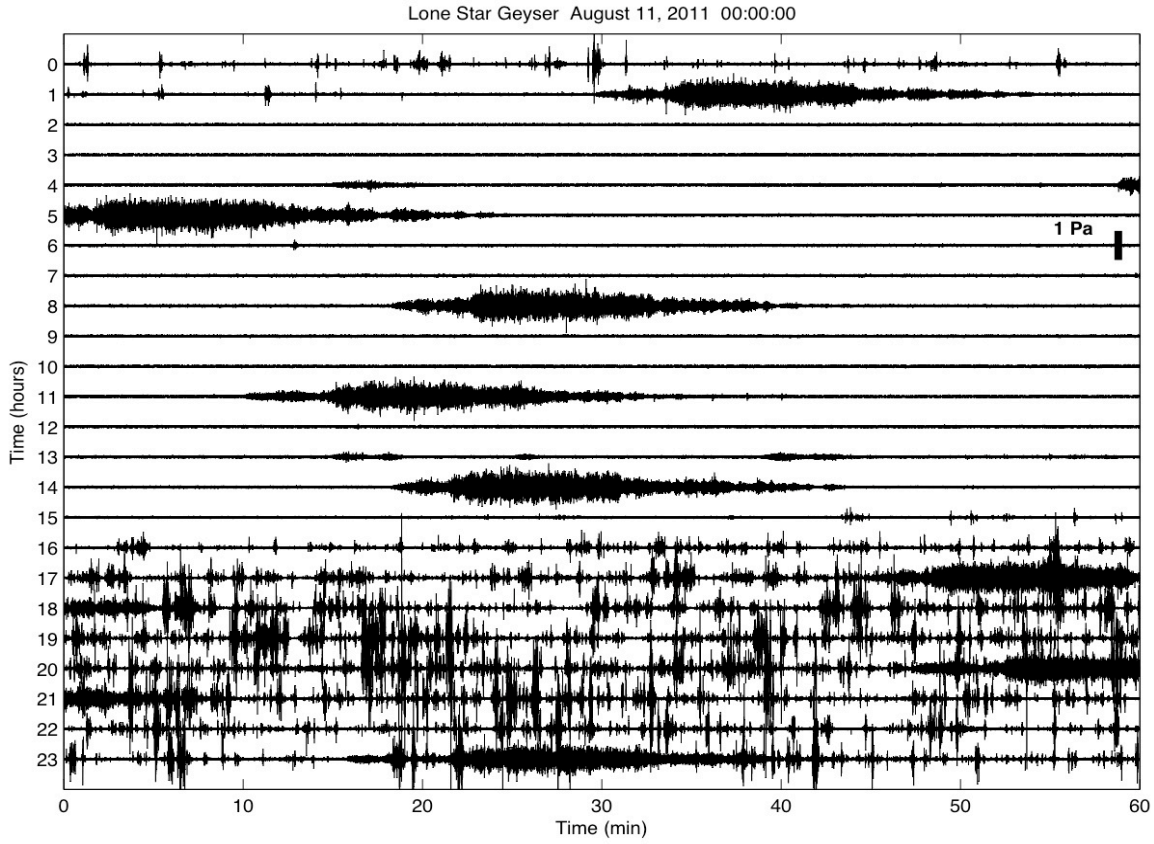

Figure 3. 24-hr helicorder from Lone Star infrasonic activity starting at 00:00:00 UTC recorded at YLS array on August 11, 2011. The cigar-shaped waveforms correspond to jet-like eruptions from Lone Star geyser. Waveforms are reduced to 1 m.

The ~ 1-hour sound from Sawmill Geyser recorded at YSM (~16 m) is manifested as a continuous waveform with amplitudes no greater than 1.6 Pa (Figure 4a). The 2-second zoomed-in interval of the original pressure trace in Figure 4d reveals a series of pulses with an average duration of 0.7 s each.

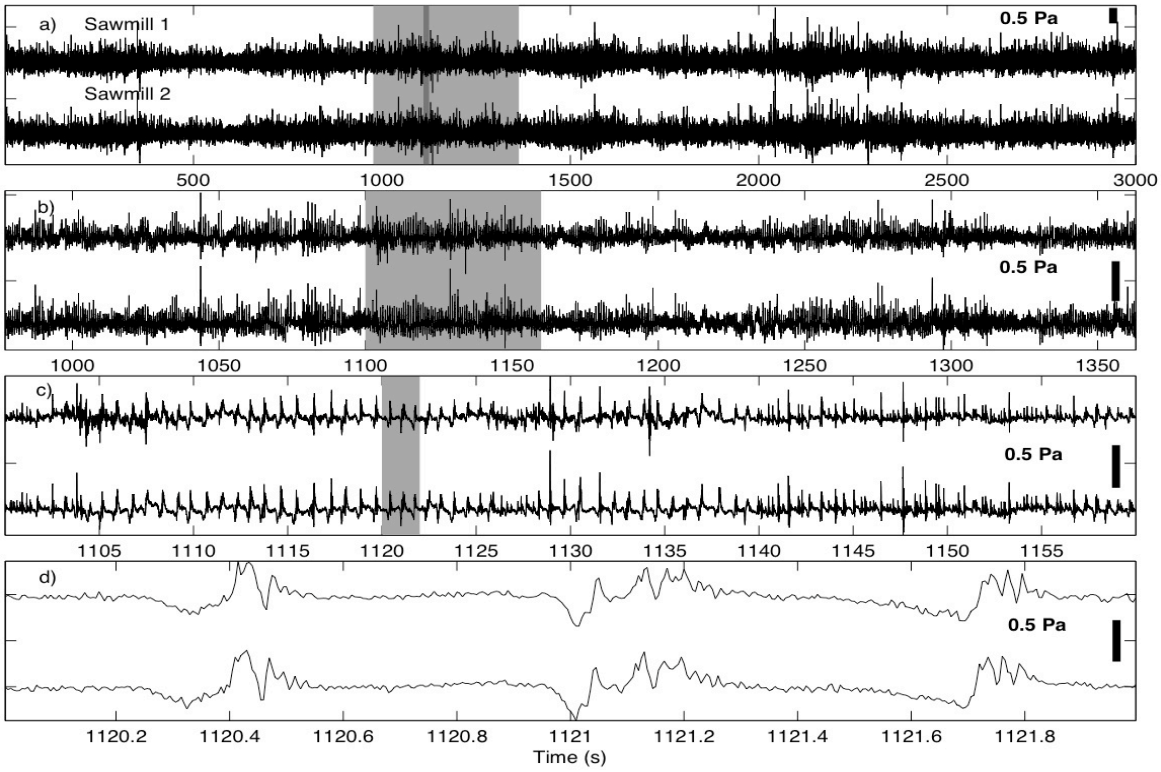

Figure 4**.** a) Sawmill's eruptive activity recorded at YSM array. Waveforms are reduced to 1 m and scale bars indicate amplitudes. The shaded boxes in a), b) and c), correspond to the 6-, 1-minute and 2-seconds zoomed-in intervals of the original pressure trace displayed in b), c) and d). The darker shaded area in a) indicates the 15 s interval selected for the analysis discussed in section 5.3

4.1 Spectral content

Power spectral density (PSD) analyses were performed on infrasonic waveforms of several eruptive events from Great Fountain and Lone Star geysers, and on a 50-minute continuous recording for Sawmill geyser (Figure 5). PSDs of background noise from each geyser were also computed in order to differentiate the spectral content of

geyser activity from that produced by noise (e.g., winds, traffic, etc). For this purpose, the averaged PSD from all the eruptions observed at one geyser was compared against the PSD of each geyser's averaged background noise. In-band geyser signal is considered as those portions of the PSD which exceed background noise by 10 dB or more. The excess pressure waveforms from each geyser were then filtered using a two-pole band-pass Butterworth filter between the in-band corners discussed below (vertical dashed lines in Figure 5a, b and c). Spectrograms were also computed to illustrate the spectral content of each geyser (Figure 6).

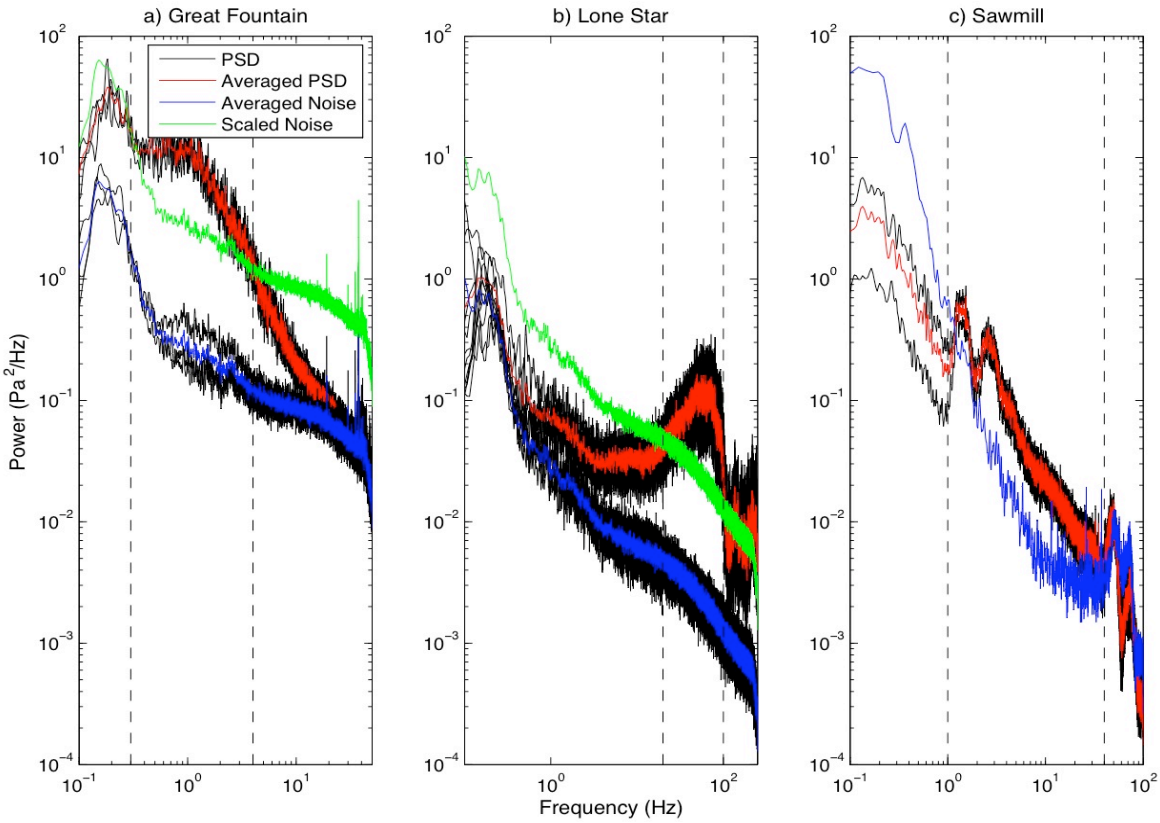

Figure 5. Power spectra from a) Great Fountain, b) Lone Star, and c) Sawmill geysers. Black lines correspond to Power Spectral Density (PSD) estimates from eruptive events (top) and background noise levels (bottom). The red line represents the averaged PSD from the eruptions at each geyser, whereas the blue line corresponds to the PSD of the averaged noise. The green line shown in a) and b) is the PSD of the averaged noise scaled by a factor of 10 dB, to determine the cutoff frequencies at which each geyser's infrasonic signal had to be filtered.

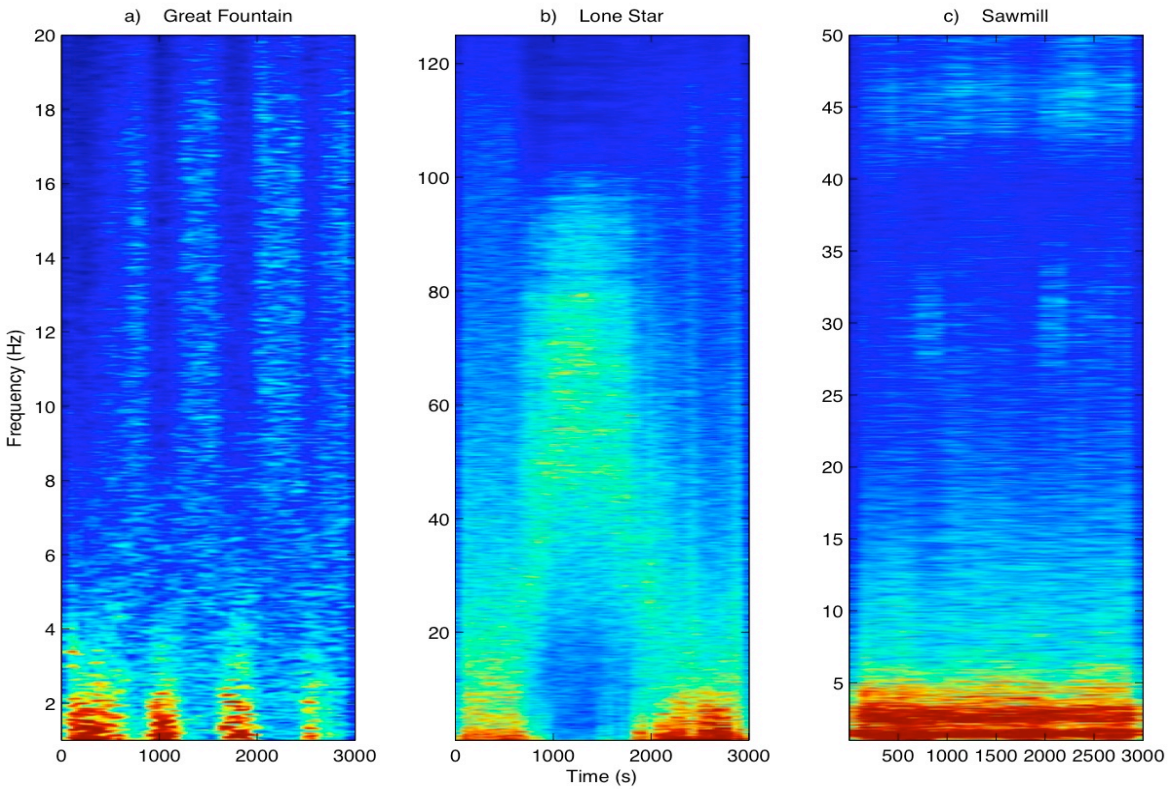

Figure 6. 50-minute spectrograms from a) Great Fountain, b) Lone Star and c) Sawmill geysers. Spectrograms were calculated using 60 s moving windows with an 8% overlap and display linear values relative to the most intense pixel in the corresponding color map for each geyser.

In Figure 5a, it can be observed that the spectral content from Great Fountain geyser's eruptions, compared against the background noise, is located between 0.3 - 4 Hz (see also Figure 6a). At Lone Star geyser, the averaged PSD from the activity displays a dramatic increase in power within the range 20 – 100 Hz. (Figure 5b). The spectrum drops abruptly at frequencies outside this range. This increase is not present in the PSD of scaled averaged noise, strongly suggesting that every eruption at Lone Star generates sound within the frequency range mentioned above. The same frequency band can also be observed in the spectrogram in Figure 6b. At Sawmill, the averaged PSD shows two peaks at 1.4 Hz and 2.6 Hz that are absent in the PSD from the background noise (Figure

5c). These two peaks are related to the ongoing eruption and will be discussed in the following section. The averaged PSD and spectrogram (Figure 6c) show that the frequency content of Sawmill lies within the range 1 – 40 Hz. The peak in power below 0.3 Hz observed at Great Fountain, Sawmill and Lone Star geysers (Figures 5 and 6) corresponds to ambient infrasound noise including ocean wave generated microbaroms.

4.2 Acoustic power

I determined the acoustic power from eruptions recorded at Great Fountain (August 10, 14:08:00 UTC), Sawmill (August 16, 15:27:50 UTC), and Lone Star (August 10, 02:24:00 UTC) geysers. The total radiated acoustic power *W* was calculated by time-integrating the squared excess pressure trace *ΔP*, and assuming a source that radiates acoustic waves radially into a hemispherical half space (Johnson, 2003):

$$W = \frac{2\pi r^2}{\rho_{air} c} \int \Delta P^2 dt \qquad \text{Eqn. (1)}$$

Where *r* is the distance between source and receiver in m, *c* is the sound speed (343 m/s at standard temperature and pressure (STP)), and ρ_{air} is the air density (0.9831 kg/m^3 at an elevation of 2233 m asl).

The August 10, 2011 eruption recorded at Great Fountain possessed a peak acoustic power value of 6.82 W during its most intense stage (see Figure 7a, b). In contrast, Sawmill's August 16, 2011 eruption exhibited the lowest acoustic power values, with an average of 0.19 W throughout the eruptive episode, and a maximum value of 0.057 W (Figure 7c, d). The acoustic power calculated from the August 10, 2011 eruption

at Lone Star (Figure 7e, f), reached a maximum value of 0.42 W as the jetting became more violent. The radiated acoustic powers calculated for the three eruptions represent characteristic values for those different eruptions and may be useful to qualitatively describe the overall acoustic intensity of an eruptive episode.

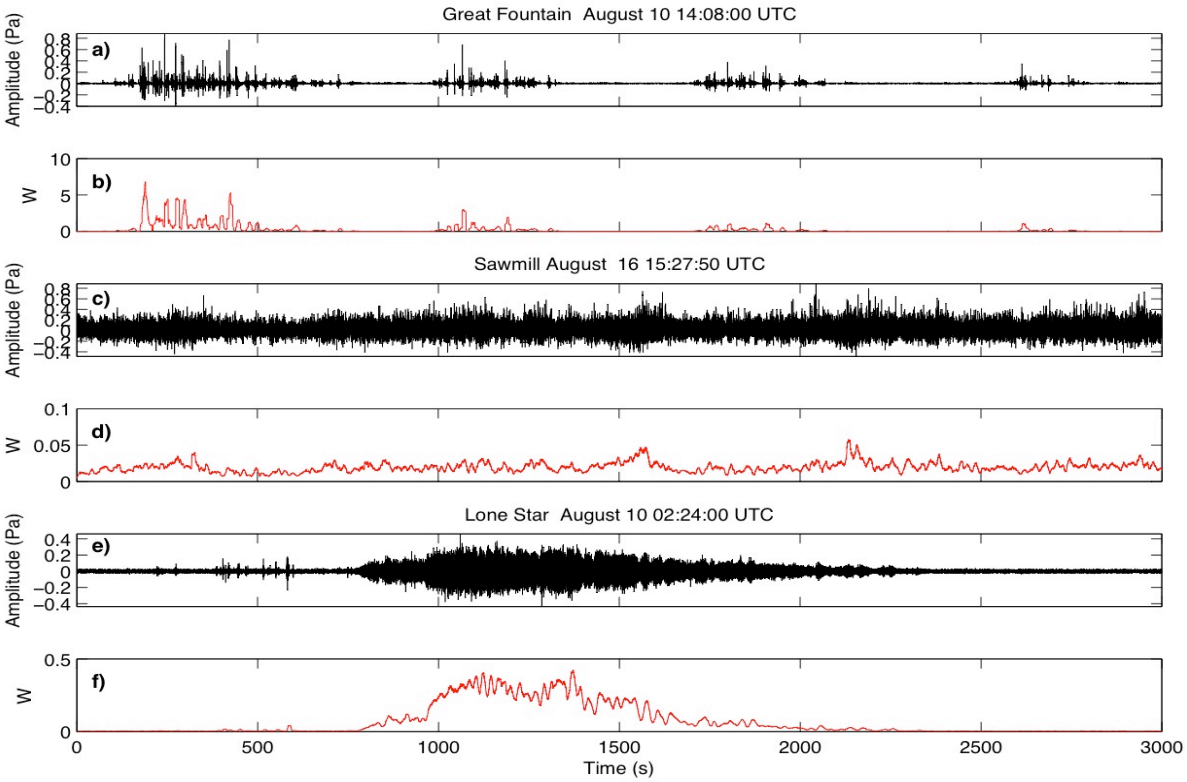

Figure 7. Acoustic power from the eruptions recorded at Great Fountain (b) on August 10, 2011, Sawmill (d), on August 16, and Lone Star (f) on August 10. A running average using a 10 s window was performed on the acoustic power trace.

5. INTERPRETATION OF INFRASOUND RADIATED FROM GEYSERS

This section provides basic analyses of the recorded infrasound waveforms from the three geysers. I model these waveforms to quantify the gas volume expelled during the August 11, 2011 eruptive episode recorded at Great Fountain geyser, Lone Star's jetting behavior, and develop a model of periodic bubble collapse for Sawmill's activity. My analysis is facilitated by video observations of the eruptions at each geyser.

5.1 Lone Star's eruption

A typical ~ 25-minute eruption from Lone Star geyser recorded on August 9, 2011 was recorded both by the infrasound array and on video. The frequency spectra from the infrasound records indicate that the low frequency content from background noise prior to the eruption, and shown in the spectrogram in Figure 8, increases to a range between 20 – 60 Hz ~2 minutes after the onset of the eruption, which consisted of spurts of water. The increase in the spectral content is visually correlated with the beginning of the jetting of water accompanied by steam, where the former is the predominant phase. An increase in absolute infrasound amplitude of about 0.03 Pa in the excess pressure waveform is also coincident with the onset of the jet (Figure 8), and this heightened amplitude remains stable for almost 300 s. During this initial stage of the eruption the energetic jet reaches a velocity of 12.5 m/s (Figure 9c). About 5 minutes after the onset of the eruption, the amount of ejected steam gradually increases with respect to the still

predominant water phase. Pressure amplitudes rise up to a peak value of ~ 0.07 Pa and the velocity of the jet increases up to 18.4 m/s (Figure 9c). This appears to coincide with the transition of the two-phase mixture, where steam is now dominant (Figure 9a). In addition, the frequency band of the acoustic signal rises from 20 – 60 Hz to 40 – 85 Hz (Figure 8) and drops back to 20 – 60 Hz as the amplitude of the waveform and jet velocity decrease. Pulsating jetting, comprised mostly of steam and a minimal amount of water, characterizes the final stage of the eruption. Pressure amplitudes gradually decay to background noise levels as the eruption comes to an end.

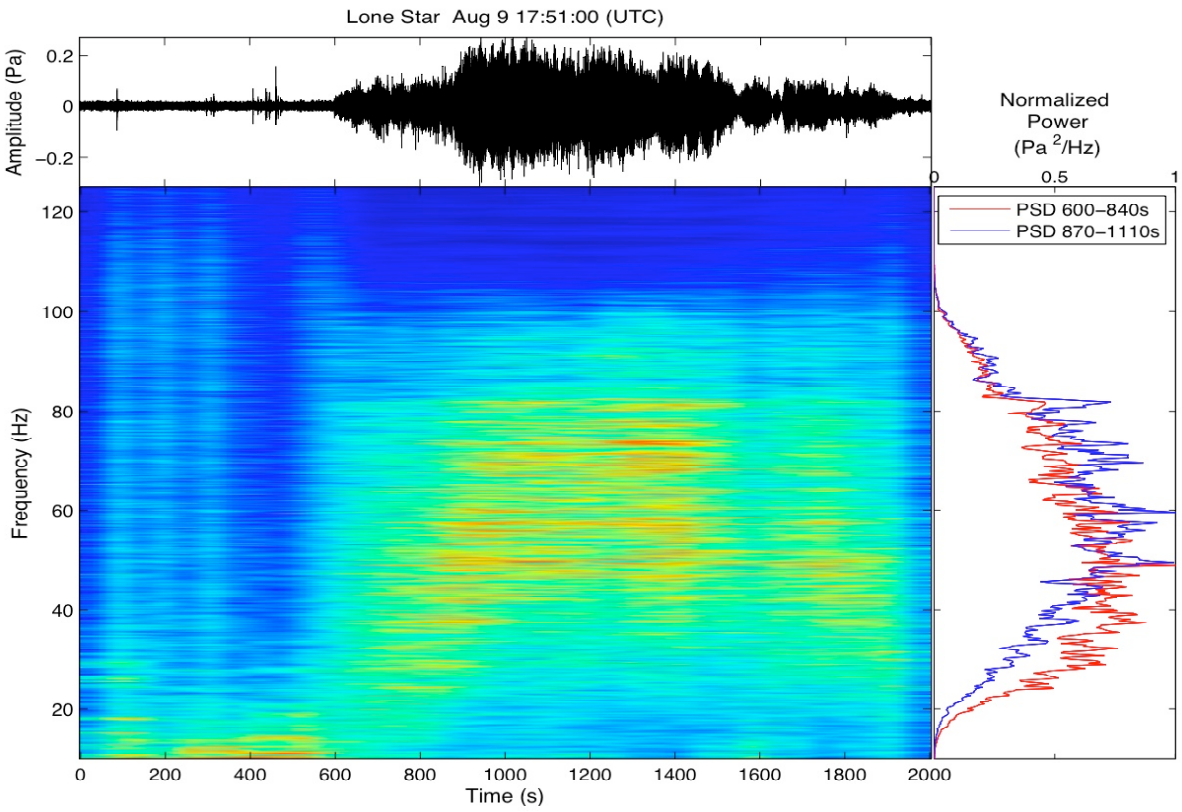

Figure 8. Spectrogram (center) and power spectral density (right) from Lone Star's eruption from August 9, 2011 at 17:51:00 (UTC). The red and blue lines represent the power spectral density (PSD) computed at two different time intervals: 600 – 840 s and 870 – 1110 s respectively. Time intervals were chosen upon observations of change in amplitude on the excess pressure amplitude. The PSD in blue shows a rise in the frequency content as the amplitude increases. This behavior can also be observed in the spectrogram.

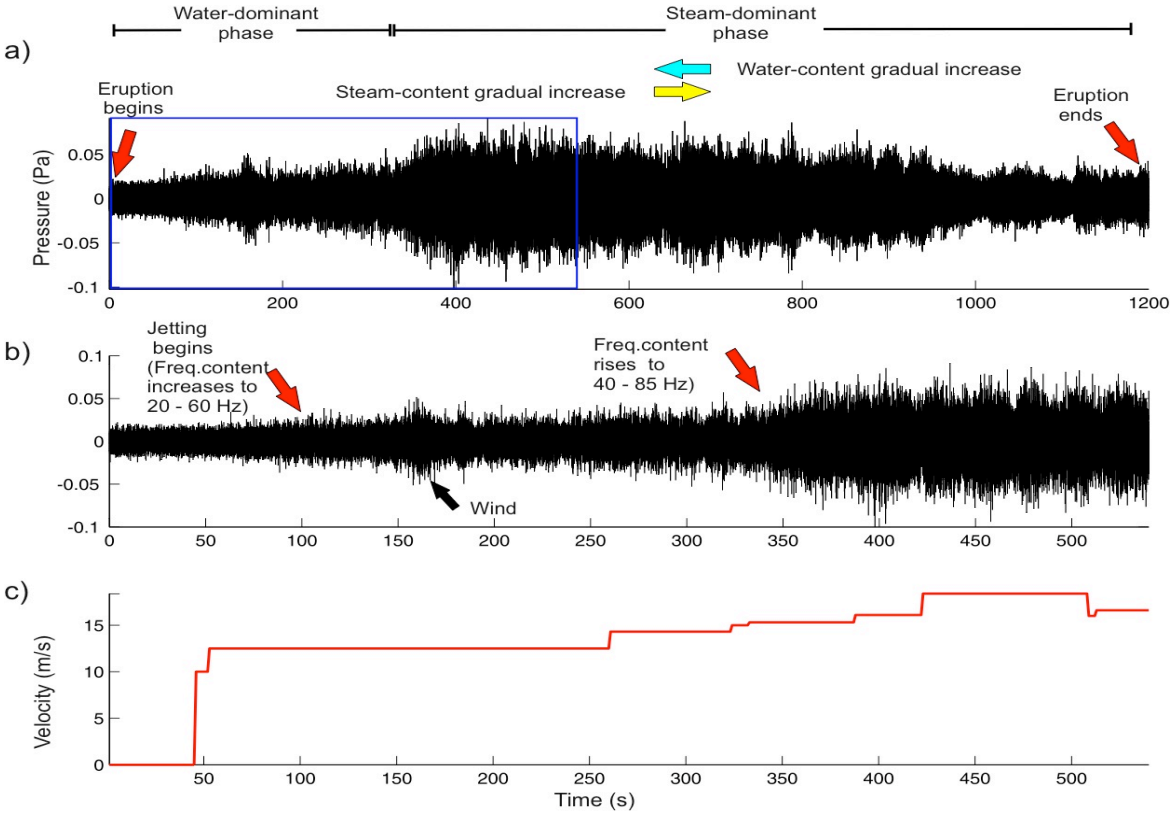

Figure 9. Jet velocity increases as the eruption at Lone Star on August 9, 2011 at 17:51:00 (UTC) develops. The amplitude in the excess pressure trace increases as the initially water-dominant mixture evolves into a steam-dominant phase.

It is evident from infrasound recordings that a couple of minutes after the eruption onset, the mixture, composed mostly of water and some steam, accelerates and generates a compression wave that propagates into the surrounding atmosphere. The infrasound amplitudes recorded from this wave are strongly related to the sound speed of the fluid in the geyser conduit. Kieffer and Sturtevant's (1984) observations on fluid dynamics of jets generated in eruptions from volcanic and geothermal settings with a convergent nozzle above a reservoir configuration, determined that fluids of high sound speed generate stronger compression waves. Kieffer and Sturtevant's (1984) work also demonstrated that the sound speed in the conduit is higher for fluids with lower densities. Therefore, such fluids produce stronger atmospheric compression waves. Moreover, in 1977, Kieffer

found that the sound speed in pure components, such as liquid or gas, is greater than the sound speed in a two-phase fluid (e.g. water-steam mixture), due to the presence of vapor bubbles or gas, which dramatically lowers the sound speed in the liquid.

My data suggest that the strength of the compression wave recorded at YLS array may be due to variations in sound speed due to the transition from a water-predominant to a vapor-predominant phase, and the difference in density of the two mixtures (Kieffer, 1977; Kieffer and Sturtevant, 1984). Video observations of the eruption show a gradual increase in the mass fraction of vapor that is in agreement with the effect sound speed exerts on fluid flow: the velocity of sound of a water steam mixture that maintains thermodynamic equilibrium between the phases, is increased as larger amounts of steam are formed in the mixture (Kieffer, 1977). As a consequence, the two-phase, vapor-rich, high-velocity fluid produces stronger compression waves than the initial two-phase, water-rich mixture (Kieffer and Sturtevant, 1984). In addition, the spectral content of the eruption increases notably several seconds after the onset of the eruption, which is coincident with the infrasound variations in amplitude, and suggests that the sound speed of a two-phase mixture increases with increasing frequency, as observed in Kieffer's (1977) work.

I regard eruptions at Lone Star geyser as a turbulent jet because of similarity in spectral shape to those generated by aircraft jet noise (Tam, 1995). Work by (e.g. Tam and Chen, 1994; Tam, 1995; Tam, 1998; Thurow et al., 2003), has shown that noise is generated by the turbulence of the jet, and consists of two distinct components: one is generated by the fine-scale turbulence of the jet, and the other component is produced by large turbulence structures, or instability waves, that flow as Mach wave radiation (Tam

et al, 2008). Woulff and McGetchin, (1976) presented a relation between the velocity of gases released at volcanoes and acoustic pressure for monopole, dipole and quadrupole source types. Woulff and McGetchin (1976) found that dipole and quadrupole sources are related to a steady gas jet interacting with the conduit walls, and jet engine-like sources that generate noise through turbulence, respectively. Caplan-Auerbach et al. (2010) investigated velocities of erupting material at Augustine volcano from pressure records, assuming that the sound was generated by a dipole source.

Following Woulff and McGetchin (1976) and Caplan-Auerbach et al. (2010) I favor a dipole source for Lone Star geyser. The water-steam mixture flowing during the eruption strikes fixed, solid boundaries such as the cone-type geyserite walls, and gives rise to an acoustic source similar to that described as a dipole-type radiation.

My observations suggest that fluctuations in air pressure recorded at YLS array due to the velocity of the ejected fluid may be directly related to the acoustic power radiated during an eruptive event at Lone Star. Variations in the acoustic power may reflect the unsteadiness in the flow as it transitions from a water- to a steam-dominated fluid.

5.2 Great Fountain's eruption

I analyzed 20 minutes of pulsating activity from the eruption at Great Fountain on August 11, 2011 at 02:21:00 (UTC). The three pulses with the highest infrasonic excess pressures observed in the waveform at 02:22:46, 02:23:07 and 02:23:54 were selected to estimate the volume of material ejected during each pulse. A comparison of the infrasonic signal

with video observations shows that the pulses are related to violent bursts of water accompanied by a considerable amount of steam.

Based upon the linear theory of sound (Dowling, 1998), it is possible to model the infrasonic waves generated by the acceleration of the atmosphere as an isotropic expansion due to the rapid release of pressurized steam and water from each pulse. If I assume an impulsive point source radiating a radially symmetric acoustic wave field into a homogeneous atmosphere, the excess pressure caused by the volumetric expansion of a monopole source into a half space may be expressed as a function of time as (Dowling and Williams, 1983; Johnson et al., 2008):

$$\Delta P_m(r,t) = \frac{Q\left(t - \frac{r}{c}\right)}{2\pi r} \qquad \text{Eqn. (2)}$$

Where Q is the source strength quantified as the product of volumetric fluid acceleration in m^3/s^2 and fluid density ρ in kg/m^3.

I estimated the corresponding time history of the mass flux (ρm^3/s) (Figure 10 d, e, and f) for the time duration of each pulse (τ) (Figure 10 a, b, c) following the method described by Johnson (2003):

$$q(t) = 2\pi r \int_0^{\tau} \Delta P\left(t + \frac{r}{c}\right) dt \qquad \text{Eqn. (3)}$$

The cumulative mass flux (ρm^3) (Figure 10 g, h, and i), which represents the integrated mass flux history (volume history), is determined by time-integrating the mass flux rate (Johnson, 2003):

$$M(t) = \int_0^{\tau} 2\pi r \left[\int_0^{\tau} \Delta P\left(t + \frac{r}{c} \right) dt \right] d\tau \qquad \text{Eqn. (4)}$$

The cumulative explosive mass flux is an important parameter for characterization of the volumetric displacement of the atmosphere due to ejection of gas and condensed phases (Johnson et al., 2008). In this work, I converted the cumulative mass flux obtained from each pulse into volume associated with the erupted fluid. Such values were achieved dividing the cumulative explosive mass flux by ρ_{air} defined in Section 4.2.

Prior to the computation of the volume history from each pulse, I filtered the infrasound waveforms using a causal and an acausal two-pole band-pass (0.3 – 4 Hz) Butterworth filter in order to assess the effects of each filter on the resultant cumulative mass flux calculations. The filters were applied on 61-, 91- and 71-second windows. These time intervals correspond to the duration of the first, second, and third pulse.

A comparison between the cumulative mass flux curve obtained from the filtered infrasound waveform using the causal filter, and the cumulative mass flux curve calculated form the filtered infrasound waveform using an acausal filter, showed that the values from the former were underestimated by 54, 48, and 46% for the first, second, and third pulses. I observed that the cumulative mass flux values from the unfiltered waveform were significantly closer to those computed from the waveform when an acausal filter was used. For this reason, I decided to apply an acausal filter to my data.

Variations in the intensity of the radiated sound from the three pulses (peak values of 0.25, 0.58, and 0.72 Pa in Figure 10 a, b, c) are evident in the infrasound records. Respective ejection volumes measured from each pulse had values of 9.60, 52.96, and 32.91 m^3.

The cumulative mass flux indicates that the second and third pulses have greater values (Figure 10 h, and i). The highest values observed during the second pulse correspond to a greater mass of displaced air with a volume that is equivalent to the amount of water and steam ejected. Notably, the third acoustic pulse displays the greatest pressure amplitudes in the infrasound record but not in the mass flux history trace (Figure 10 c, and i), suggesting a more impulsive, short-lived ejection with a lesser amount of erupted flux. Video recordings from the three pulses are provided as Supplementary materials with an annotated hemispherical overlay corresponding to the volumetric source time history inferred from the infrasound.

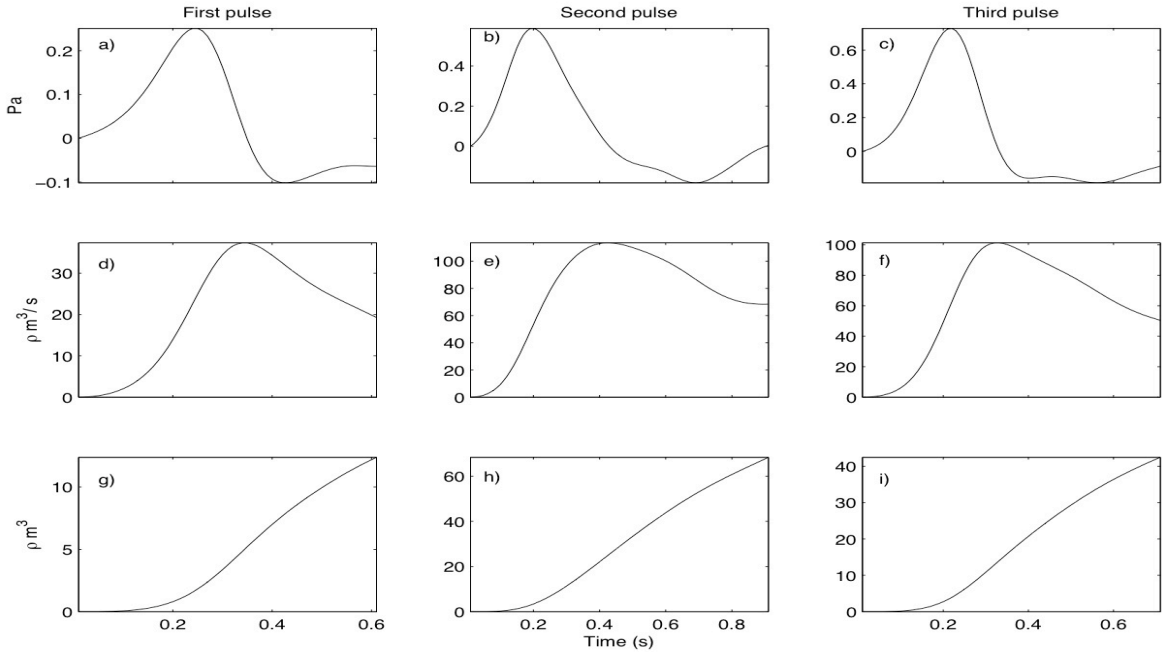

Figure 10. Pressure trace, mass flux and cumulative flux of the first pulse (a, d, g) from the final eruptive stage at Great Fountain (02:21:00 UTC, on August, 11, 2011. Second pulse (b, e, h), and third pulse (c, f, i) are also shown here.

5.3 Sawmill's eruption

In order to identify a high signal-to-noise interval from the ~50 minute recordings I performed a cross correlation between the infrasound waveforms from the two spatially separated microphones. I found a 15 second-long time interval (Figure 4a) with a high signal-to-noise ratio in which the normalized cross correlation value was 0.96. Here, I observed 19 pulses occurring periodically at 0.7 second-long intervals (Figure 11).

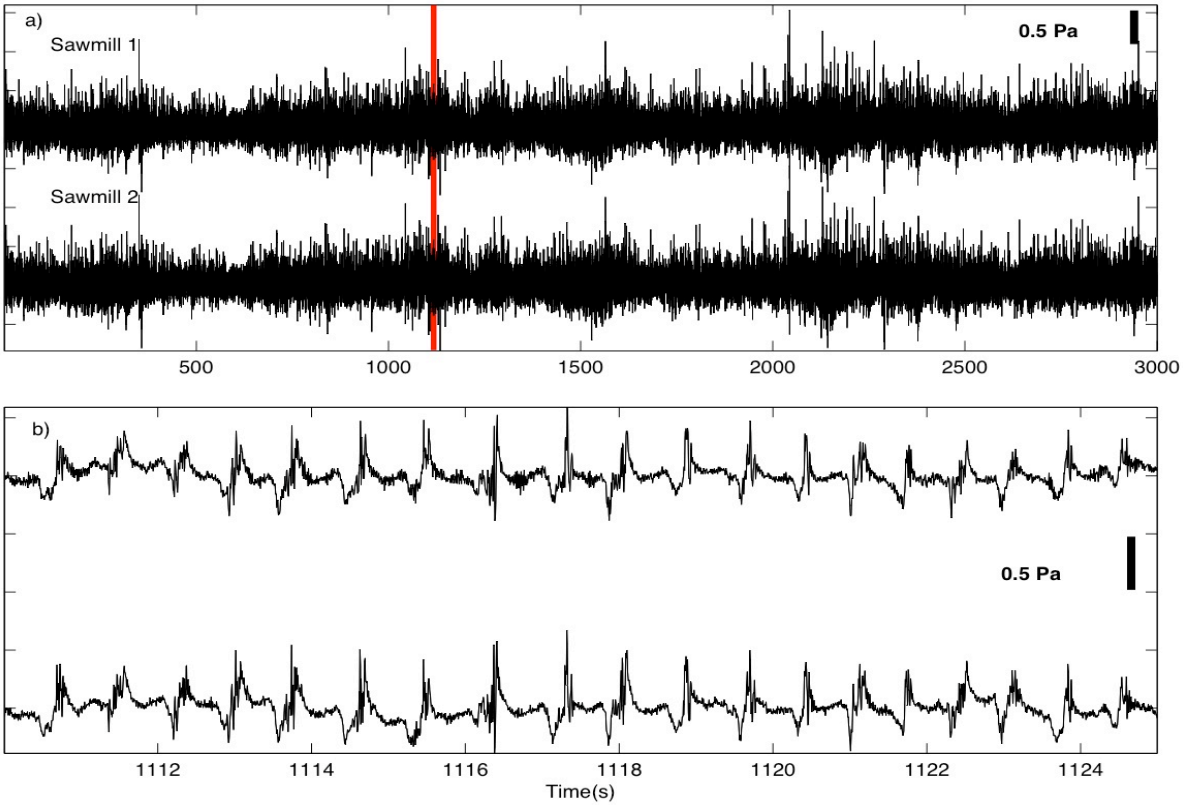

Figure 11. 15-s interval from the 50-minute eruption recorded at Sawmill chosen for analysis. The time interval is indicated with a red bar in a). b) Zoomed-in 15-s interval. The 19 pulses were stacked and filtered below 30 Hz for the analysis.

The 19 pulses were stacked and filtered below 30 Hz to determine a characteristic waveform representative of all pulses. The characteristic waveform (Figure 12a) begins with a ~ 0.25 s rarefaction followed by a ~0.33 s compression. Moreover, high frequency

contributions become evident at ~0.02 s following the zero crossing of the bimodal pulse: three peaks are observed at 0.34, 0.38, and 0.42 s (Figure 12a). A PSD of the waveform stack and all the 19 pulses (Figure 12b) also displays the same three peaks at 30, 49 and 74 Hz, as observed on the characteristic waveform. The spectrogram from the stacked unfiltered infrasound waveform, computed to investigate the frequency evolution of the pulse with respect to time (Figure 13), shows contributions related to the fundamental frequency of the characteristic waveform at 1.42 Hz, as well as the peaks observed at the stacked PSD. The presence of the three peaks in Figures 12a, 12b, and 13 suggest that the sound is generated by the source, and not by transient instabilities in the flux.

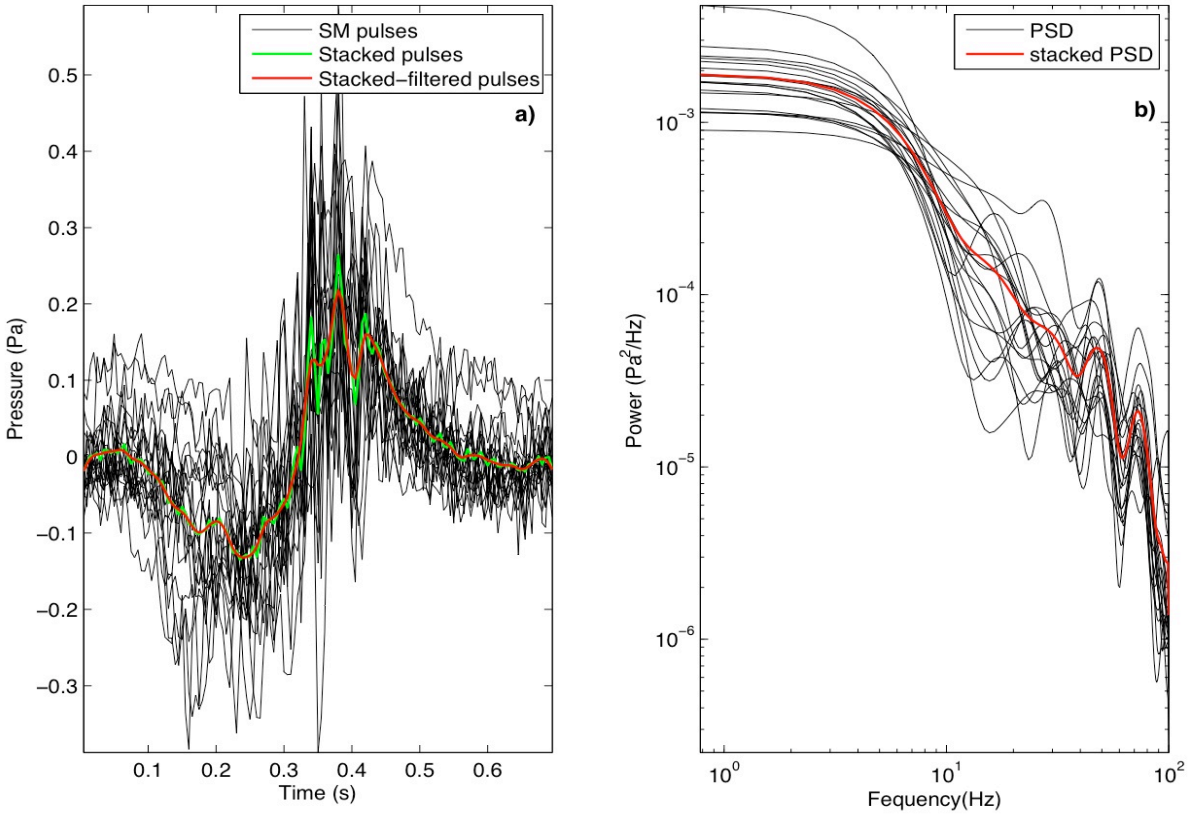

Figure 12. a) Infrasound from the 19 pulses (black lines) comprised in the 15 s interval from Sawmill eruption (August 16, 2001) selected for analysis. The 19 pulses were stacked (green line) and filtered below 30 Hz (red line) to determine a characteristic waveform. b) PSDs were calculated for each pulse (black lines) and stacked (red line).

Video taken of the eruption sequence (Supplementary Materials) shows that the increase in frequency coincides with the visible ejection of water and steam, and is probably related to the bursting of steam bubble(s) near the surface. This phenomenon is similar to what has been observed and documented on some Strombolian explosions and in laboratory experiments, where a bursting bubble at the surface of a lava column generates sound waves with a high-frequency content (Vergniolle and Brandeis, 1994; Vergniolle and Brandeis, 1996, Vidal et al., 2006).

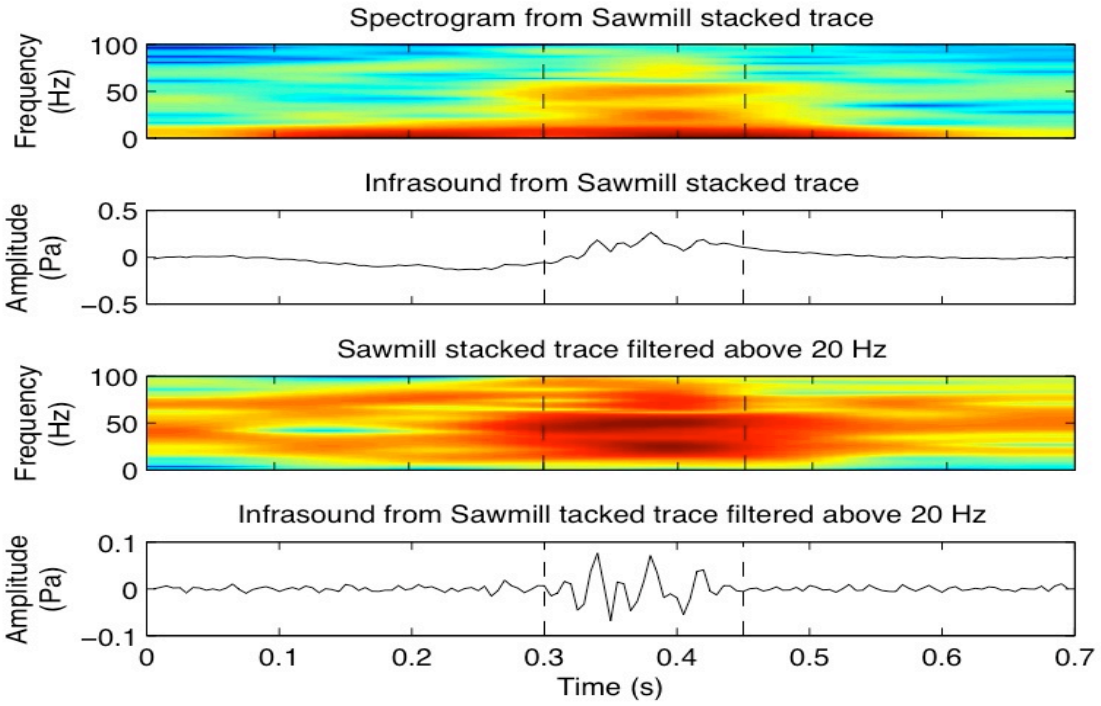

Figure 13. Spectrograms and acoustic pressure traces computed for the unfiltered stacked trace (top panels) and stacked trace filtered above 20 Hz (bottom panels). The three peaks observed on both infrasound traces correspond to sound generated by the source.

Conjoint infrasound and video records of the periodic bursts of water and steam suggest that the source can be modeled as a volumetric source with dimension that is small with respect to the radiated infrasound wavelengths (Eqn. 2). I attempt to model both the periodic bursting of steam bubbles and presumed bubble collapses as acoustic

monopole sources at the free surface. The process repeats itself thousands of times producing an infrasonic harmonic tremor.

Following Eqns. 3 and 4 the mass flux and mass flux history (Figure 14 b, c) were determined for the characteristic waveform (Figure 14a), which was filtered below 10 Hz for cleaner analysis of low-frequency motions. The mass flux history was also computed for the 19 individual pulses and compared against video. In the video sequence where the mass flux history was incorporated (see Supplementary Materials), I observed that the periodic increase in the values of the cumulative flux curve were related to an ejection of a mass of water and steam from the nozzle, as it expanded, the released material displaced the atmosphere outwards. The decreasing values in the cumulative flux curve corresponded to the instant when all the erupted mixture had already left the nozzle. A decrease in the water level of the pool during this stage occurred simultaneously (The reader is encouraged to look at the video of the eruption provided in the Supplementary Materials section).

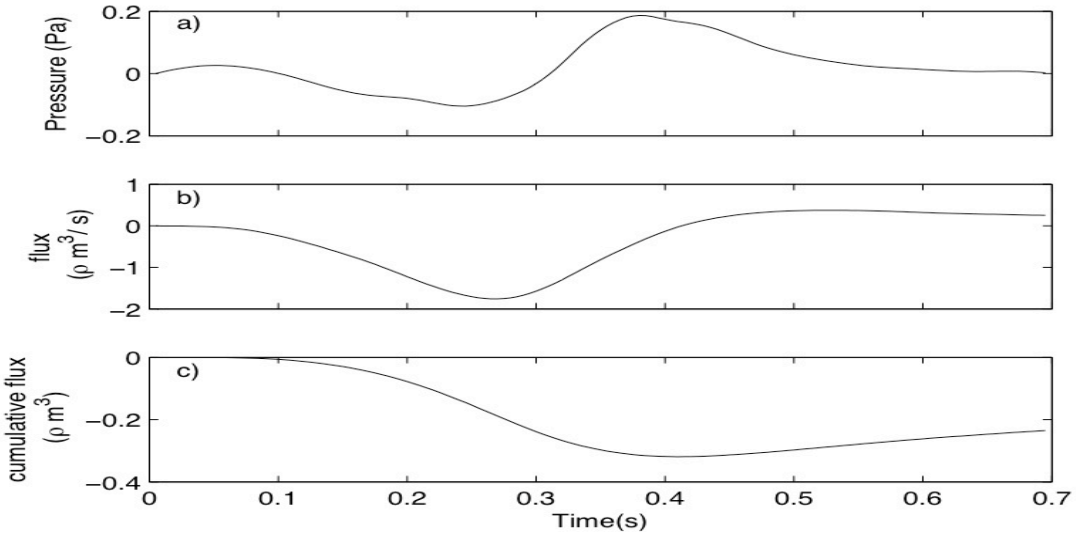

Figure 14. a) Infrasound record from the characteristic waveform, b) Time history of the mass flux, and c) Cumulative mass flux.

I propose a model for the eruptive cycles of Sawmill geyser based on the video, infrasound recordings and volume history results (Figure 15). According to observations from previous studies on geyser activity (Kieffer, 1984; Kieffer, 1989; Kedar et al., 1996; Bryan, 2008), water in a geyser plumbing system is heated beyond the local boiling point due to heat conduction from hot wall rocks. Steam bubbles form and rise and either condense and collapse as they rise through the system and heat the cooler water nearer the surface or expand due to decreasing hydrostatic pressure. As steam flux increases and conduit water is heated bubbles continue to rise and may coalesce into a larger steam slug. This phenomenon is suggested in Figure 15a where a subtle pressure increase is evident at about 0.1 s. The steam slug completes its ascension and reaches the surface. Shortly after, it forms a spray dome, which is a mound of water that is thrown up into the air (Weston, 1960). The spray dome ejects considerable amounts of water and steam into the free surface, which in turn generate a compression acoustic wave that displaces the surrounding atmosphere. The peak in the infrasound waveform at almost 0.4s denotes this behavior (Figure 15b). The dramatic decrease represented by the minimum value in the cumulative flux curve, may be due to the sudden release of the steam in the gas slug that was confined by the surrounding water column (Figure 15b). A new gas slug forms and as it continues its way up to the surface, the surrounding hydrostatic conditions of the system (Kieffer, 1984) allow it to undergo a new expansion, denoted by the increase in amplitude of the infrasound and cumulative flux waveforms (Figure 15c). The whole process duration is 0.7 s, and it repeats continuously, generating the series of pulses observed in the infrasound from Figure 11 until the eruptive stage dies off.

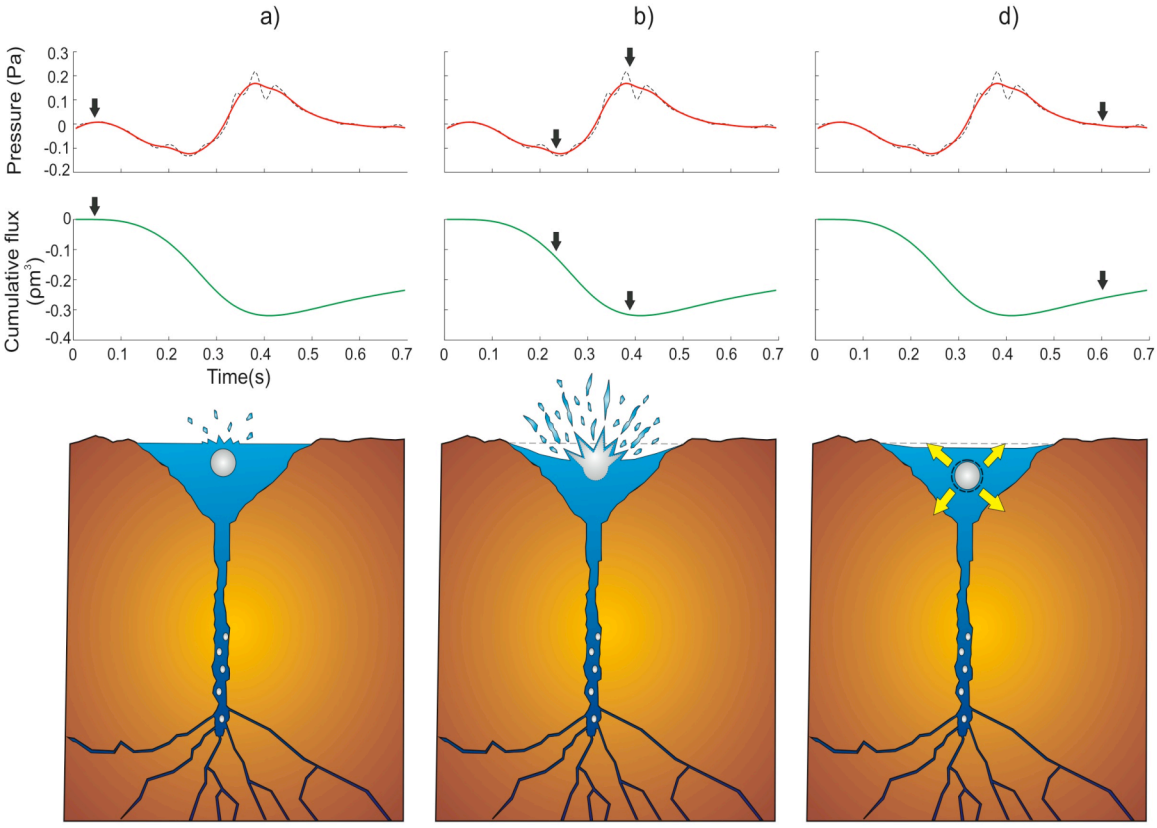

Figure 15. Source model proposed for Sawmill (not on scale). The acoustic pressure traces include the characteristic wave filtered below 10 Hz (continuous red line) and 30 Hz (dashed line).

6. FINAL REMARKS

From the three geysers analyzed in this work, Great Fountain reaches the greatest heights (~ 45 m) during the initial phase of an eruptive episode, followed by Lone Star geyser (~ 14 m). In contrast, Sawmill displays eruptions that are only a few meters in height. The pressure amplitudes from the sound recorded at Great Fountain (Figure 2) are also greater than the amplitudes from Lone Star and the 50-minute interval recorded at Sawmill. However, the highest-pressure amplitudes are confined to the initial stage of the eruption at Great Fountain and diminish substantially with each stage. Pressure amplitudes from infrasound recorded at Lone Star also display the highest values during its most intense eruptive phase, whereas the amplitudes observed at Sawmill remain constant throughout the eruption (Figure 4). Similarly, the comparison between the acoustic power calculated from the eruptions recorded at the three geysers, and discussed in section 4.2 (Figure 7), indicates that the greatest acoustic intensity is present at Great Fountain during its initial eruptive phase comprised of a considerable amount of steam, suggesting a vigorous onset that decays as the eruption develops. Lone Star's acoustic power is less vigorous than that observed at Great Fountain. As steam displaces water in the water-steam mixture, column height and acoustic radiation increases in intensity. Conversely, the lowest acoustic power is present at Sawmill; however, it does not undergo significant changes during the eruptive event. My data and video observations

from these three geysers suggest that the difference in the intensity of radiated acoustic energy is related to 1) eruption dynamics: the more intense activity and greatest heights were generated by the two geysers (Great Fountain and Lone Star) where a considerable amount of fluid was discharged in a brief amount of time, contrary to a continuous fluid discharge, as observed at Sawmill. In addition, the infrasound intensity seems to be greater for fountain-type geysers than for cone-type geysers. This observation agrees with the results obtained by Johnson, et al. (subm) related to infrasound radiated from both types of geysers located at Yellowstone National Park; and 2) the varied physical characteristics of the geysers: vent geometries and possible temporary obstructions in the conduit during eruptions (e.g. Lone Star) that may affect the fluid ejection, therefore, modifying the frequency content of the acoustic source (Figure 5).

Finally, the infrasound waveforms from the fountain-type geysers (Great Fountain and Sawmill) differ notably from the infrasound recorded at cone-type geysers (Lone Star). The former are characterized by a series of pulses present throughout the eruption, whereas the latter displays a continuous and emergent waveform. The different acoustic behavior may be related to the presence of a sinter mound at cone-type geysers where the sound generated by the moving fluid may be influenced by resonant organ pipe effects along the vent tube.

Eruption mechanisms from these geysers provide good insight on volcanic eruptive processes (Kieffer, 1984) since they are good analogues for the study of volcanic eruptions.

7. CONCLUSIONS

Acoustic monitoring using infrasound arrays facilitates the characterization of eruptions generated by cone-type and fountain-type geysers. My study on infrasound waveforms and their spectral content, along with the acoustic energy and video observations obtained from eruptions registered at Great Fountain, Lone Star and Sawmill geysers, provides useful insight on acoustic intensity of the eruptions, episodicity in fountain-type geysers, duration of eruption cycles, amount of erupted fluid during an eruption, and the different eruptive mechanisms associated to different eruption styles, which in turn, promote better comprehension of dynamic processes that involve the ejection of two-phase fluids. In this study, I have shown that the intensity of the infrasound radiated during an eruption is strongly affected by the type of geyser, i.e. infrasound sources from fountain-type geysers appear to provide greater radiation than sources from cone-type geysers. The sound velocity of the fluid, which is controlled by its density, also affects infrasound intensity.

Based on my findings from this work, and from previous studies on variations in geysers periodicity and behavior (Ingebritsen and Rojstaczer, 1993; Ingebritsen and Rojstaczer, 1996; Rojstaczer et al., 2003; Hurwitz, et al., 2008), I recommend a continuous analysis and video observations of the properties of geysers and their processes in order to gather enough information, and better understand the conditions required in multiphase systems prior and during an eruption.

REFERENCES

Arrowsmith, S.J., Johnson, J.B., Drob, D.P., and Hedlin, M.A.H., 2010. The seismoacoustic wavefield: a new paradigm in studying geophysical phenomena. Rev. Geophys. 48, RG4003.

Bryan, T.S., 2008. The geysers of Yellowstone, 4th edition. University Press of Colorado, Niwot, CO, 463 pp.

Caplan-Auerbach, J., Bellesiles, A., Fernandes, J.K., 2010. Estimates of eruption velocity and plume height from infrasonic recordings of the 2006 eruption of Augustine Volcano, Alaska. J. Volc. Geotherm. Res. 189: 12 – 18.

Cole, R.H., 1948. Underwater explosions, Princeton University Press. USA. Pp. 464.

Dowling, A.P. 1998. Steady-state radiation from sources, in Handbook of Acoustics, ed. M. Crocker, pp. 99 – 117, John Wiley, Hoboken, N.J.

Dowling, A.P., and Williams, J.E.F., 1983. Sound and Sources of sound. Ellis Horwood Limited, Chichester, p. 321.

Drob, D.P., and Picone, J.M., 2003. Global morphology of infrasound propagation, J. Geophys. Res. 108, D21, 4680, doi: 10.1029/2002/JD003307.

Garces, M.A., Hansen, R., and Lindquist, K.G., 1998. Travel times for atmospheric waves propagating in a stratified atmosphere, Geophys. J. Int. 135, 255 – 263.

Garces, M. A., Harris, C. Hetzer, J.Johnson, S. Rowland, E, Marchetti, and P. Okubo. 2003. Infrasonic tremor observed at Kilauea volcano, Hawai'i, Geophys. Res. Let., 30(20), 2023, doi:10.1029/2003GL018038.

Hurwitz, S., Kumar, A., Taylor, R, and Heasler, H., 2008. Climate-induced variations of geyser periodicity in Yellowstone National Park, USA.

Hutchinson, R.A., Westphal, J.A., and Kieffer, S.W., 1997. In situ observations of Old Faithful Geyser, Geology, 25, 875 – 878. Doi:10.1130/0091-7613(1997)025<0875

Ingebritsen, S.E. and Rojstaczer, S.A., 1993. Controls on geyser periodicity. Science, 262(5135): 889 – 892.

Ingebritsen, S.E. and Rojstaczer, S.A., 1996. Geyser periodicity and the response of geysers to deformation. J. Geophys. Res. 101, B10, 21,891 – 21,905.

Johnson, J.B., 2003. Generation and propagation of infrasonic airwaves from volcanic explosions, J. Volc. Geotherm. Res., 121(1-2), 1 – 14.

Johnson, J.B, and Lees, J.M., 2000. Plugs and chugs – seismic and acoustic observations of degassing explosions at Karymsky, Russia and Sangay, Ecuador. J. Volc. Geotherm. Res. 101(1-2), 67 – 82.

Johnson, J.B., Aster, R.C., and Kyle, R. Philip. 2004. Volcanic eruptions observed with infrasound. Geophys. Res. Lett., 31(L14604):doi:10.1029/2004GL020020.

Johnson, J.B., Aster, R., Jones, K. R., Kyle, P., and McIntosh, B., 2008. Acoustic source characterization of impulsive Strombolian eruptions from the Mount Erebus lava lake. J. Volc. Geotherm. Res. 177, 673 – 686.

Johnson, J.B., Anderson, J., Quezada-Reyes, A., and others, in prep. Detecting geyser activity using infrasound, J. Volc. Geotherm. Res.

Kedar , S., Kanamori, H., 1998. Bubble collapse as the sources of tremor at Old Faithful Geyser, J. Geophys. Res. 103, B10, 24283 – 24299.

Kedar, S., Sturtevant, B., and Kanamori, H.,1996. The origin of harmonic tremor at Old Faithful Geyser, Nature, 379, 708 – 711.

Kieffer, S.W., 1977. Sound speed in liquid-gas mixtures: water-air and water-steam. J. Geopys. Res. 82: 2895 – 2904.

Kieffer, S.W., 1984. Seismicity at Old Faithful geyser: an isolated source of geothermal noise and possible analogue of volcanic seismicity. J. Volcanol. Geotherm. Res. 22: 59 – 95.

Kieffer, S.W., 1989. Geologic nozzles, Rev. Geophys. 27, 3 – 38.

Kieffer, S.W. and Sturtevant, B., 1984. Laboratory studies of volcanic jets. J. Geophys. Res. 89: 8253 – 8268.

Lighthill, M.J. 1952. On sound generated aerodynamically: I. General theory. Proc. Roy. Soc. London Ser. A, 211, 564 – 581.

Marcillo, O., and Johnson, J.B., 2010. Tracking near-surface atmospheric conditions using an infrasound network, J. Acoust. Soc. Am. 128(1), EL 14 – 19.

Marcillo, O., Johnson, J.B. and Hart, D., 2012. Implementation, characterization, and evaluation of an inexpensive low-power low-noise infrasound sensor based on a micro-machined differential pressure transducer and a mechanical filter. J. Atmos. Ocean. Tech.

Rinehart, J.S., 1970. Heat flow from natural geysers. Tectonophys. 10, 11 – 17.

Ripepe, M., Marchetti, E., Ulivieri, G., 2007. Infrasonic monitoring at Stromboli Volcano during the 2003 effusive eruption: insights on the explosive and degassing process of an open conduit system. J. Geophys. Res. Solid Earth 112.

Rojstaczer, S., Galloway, D.L., Ingebritsen, S.E., and Rubin, D.M., 2003. Variability in geyser eruptive timing and its causes: Yellowstone National Park, Geophys. Res. Lett., 30, No. 18, doi:10.1029/2003GL017853.

Rowe, C.A., Aster, R.C., Kyle, P.R., Dibble, R.R., Schlue, J.W., 2000. Seismic and acoustic observations at Mount Erebus Volcano, Ross Island, Antarctica, 1994 – 1998. J. Volc. Geotherm. Res. 101 (1-2), 105 – 128.

Tam, C.K.W.,1995. Supersonic jet noise. Annu. Rev. Fluid. Mech., 27: 17 – 43.

Tam, C.K.W., 1998. Jet Noise: since 1952. Theoret. Comput. Fluid Dynamics, 10: 393 – 405.

Tam, C.K.W., and Chen, P., 1994. Turbulent mixing noise from supersonic jets. AIAA J. 32, 1774-1780.

Tam, C.K.W., Viswanathan, K., Ahuja, K.K. and Panda, J., 2008. The sources of jet noise: experimental evidence. J. Fluid. Mech. 615: 253 – 292.

Thurow, B., Samimy, M. and Lempert, W., 2003. Compressibility effects on turbulence structures of axisymmetric mixing layers. Phys. Fluids, 15: 1755 – 1765.

Vergniolle, S., and Brandeis, G., 1994. Origin of the sound generated by Strombolian explosions. Geophys. Res. Lett. 18, 1959 – 1962.

Vergniolle, S., and Brandeis, G., 1996. Strombolian explosions 1. A large bubble breaking at the surface of a lava column as a source of sound. J. Geophys. Res. 101(B9): 20433 – 20447.

Vidal, V., Geminard, J-C., Divoux, T., and Melo, F., 2006, Acoustic signal associated with the bursting of a soap film which initially closes an overpressurized cavity. Eur. Phys. J. B 54, 321 – 339.

Weston, D.E., 1960. Underwater explosions as acoustic sources, Proc. Phys. Soc. 76, 233– 249.

Woulff, G., and McGetchin, T.R., 1976, Acoustic noise from volcanoes: Theory and Experiment. Geophys. J. R. Astr. Soc. 45, 601 – 616.